Correspondence Authors:

Name: Guofeng Zhu [a,b,*]

Institution:

[a] *College of Geography and Environment Science, Northwest Normal University, Lanzhou 730070, Gansu, China*

[b] *Shiyang River Ecological Environment Observation Station, Northwest Normal University, Lanzhou 730070, Gansu, China*

Address:

College of Geography and Environment Science of Northwest Normal University, No.967 East Anning Road, Lanzhou, Gansu, China 730070.

Tel: +86-13909310867

E-mail: zhugf@nwnu.edu.cn

Evaporation, infiltration and storage of soil water in different vegetation zones in the Qilian Mountains: A stable isotope perspective

Guofeng Zhu [a,b]*, Leilei Yong [a,b], Zhao Xi [a,b], Yuwei Liu [a,b], Zhuanxia Zhang [a,b], Yuanxiao Xu [a,b], Zhigang Sun [a,b], Liyuan Sang [a,b], Lei Wang [a,b]

[a] *College of Geography and Environment Science, Northwest Normal University, Lanzhou 730070, China*

[b] *Shiyang River Ecological Environment Observation Station, Northwest Normal University, Lanzhou 730070, Gansu, China*

Abstract: The processes of water storage and runoff generation have not been fully understood in different vegetation zones in mountainous areas, which is the main obstacle to further understanding hydrological processes and improving water resource assessments. To further understand the process of soil water movement and runoff generation in different vegetation zones (alpine meadow, coniferous forest, mountain grassland, and deciduous forest) in mountainous areas, this study monitored the temporal and spatial dynamics of hydrogen and oxygen stable isotopes in the precipitation and soil water of the Xiying River Basin. The results show that the evaporation intensities of the four vegetation zones followed the order of mountain grassland > deciduous forest > coniferous forest > alpine meadow. The soil water in the alpine meadows and coniferous forests evaporated from only the topsoil, and the rainfall input was fully mixed with each layer of soil. The evaporation signals of the mountain grasslands and deciduous forests could penetrate deep into the middle and lower layers of the soil as precipitation quickly flowed into the deep soil through the soil matrix. Each vegetation zone's soil water storage capacity followed the order of alpine meadow > deciduous forest > coniferous forest > mountain grassland. In addition, the water storage capacity of shallow soils in different types of vegetation areas was weaker than that of deep soils. This work will provide a new reference for understanding soil hydrology in arid headwater areas.

Key words: Xiying River; Stable isotope; Drought, Soil water storage

1. Introduction

In arid inland river basins, changes in climate and vegetation will affect the hydrological cycle (Tetzlaff et al., 2013; Sharma et al., 2021). As an important part of the water cycle, soil water in the unsaturated zone can be converted from precipitation to stream or groundwater recharge. Determining soil water's evaporation, infiltration, and storage properties is critical for understanding the regional hydrological cycle and water balance under the background of climate and vegetation changes (Brooks et al., 2010; Grant and Dietrich, 2017).

Isotopes, as "fingerprints" of water, have been used to track ecohydrological characteristics, such as evaporation (Barnes and Allison, 1988; Zhu et al., 2021b), groundwater recharge (Koeniger et al., 2016), infiltration paths (Tang and Feng, 2004; Duvert et al., 2016; Zhu et al., 2021a), evapotranspiration distribution (Xiao et al., 2018; Gibson et al., 2021) and water absorption by plants (Rothfuss and Javaux, 2017).

Water seepage in the unsaturated soil zone and the water evaporation at the air–soil interface are the main forms of soil water transport. Seasonal variations in precipitation isotopes are often used to track the process of soil water leakage (Stumpp et al., 2012). During the piston infiltration process, precipitation with different $\delta^{2}H$ and $\delta^{18}O$ peaks are retained in the soil profile and gradually disappears as the infiltration depth increases (Sprenger et al., 2016a), while the preferential flow will keep these peaks until reaching the deep soil layer (Peralta-Tapia et al., 2015). During a precipitation event, the response of the water isotopes in the surface soil to precipitation is more obvious, changing to nearly that of the stable isotopes of the precipitation. With the deepening of the soil layer, the seasonal variation in precipitation isotope signals rapidly attenuates, and the influence of precipitation on soil water gradually weakens (Sprenger et al., 2017). Evapotranspiration is the main form of soil water dissipation. Because the mass of hydrogen and oxygen atoms that make up water molecules are related to their thermodynamic properties, isotope fractionation of water will occur in the process of the water cycle. The evaporation of

liquid water produces water vapor enriched in ^{1}H and ^{16}O, while the remaining water is enriched in ^{2}H and ^{18}O (Ferretti et al., 2003). Dansgaard (1964) proposed the concept of d-excess (d-excess=$\delta^{2}H$-8$\delta^{18}O$) to illustrate the intensity of evaporative fractionation. In the state of isotopic equilibrium, the d-excess is 10. Compared with d-excess, lc-excess can better explain the evaporative fractionation process. The main reason is that lc-excess of precipitation and soil water changes smoothly and has relatively small seasonal changes (Landwehr et al., 2014). The dynamic changes in isotopes record the signal of soil water evaporation. This enrichment from dynamic fractionation exists in soil water isotopes in different climatic regions. Compared with temperate regions, the signals of evaporation in arid and Mediterranean environments penetrate deeper into the soil (Sprenger et al., 2016b). Some water is stored in the soil after evaporation and seepage. The water storage capacity of humid areas is higher than that of arid areas, the water storage capacity of forests is higher than that of grasslands, and the water storage capacity of the surface soil layer is lower than that of deeper soil layers with higher clay content (Heinrich et al., 2019; Sprenger et al., 2019; Kleine et al., 2020; Snelgrove et al., 2021).

In alpine mountains, climate warming accelerates the melting of glaciers and frozen soil, and the dynamic interaction between water bodies stored in different media becomes the main influence on the water cycle (Penna et al., 2018). Previous studies on the evaporation, infiltration, and storage of soil water have mostly focused on different climatic regions or vegetation types in the same climatic region. Understanding the climatic and hydrological conditions of different vertical vegetation zones and clarifying the regulating role of vegetation in the water cycle can help better adapt to climate change's influences on the hydrological cycle in source areas. This study monitored the stable isotope composition of precipitation and soil water and the spatiotemporal dynamics of soil water storage in four vegetation zones (alpine meadow, coniferous forest, mountain grassland, and deciduous forest) with different hydrothermal conditions in the Xiying River Basin. To explore the differences in soil water evaporation, infiltration, and storage processes in these four different climates, vegetation types, and terrain types, the following research

objectives were proposed: (1) to explore the evolution of isotope evaporation signals and the "memory effects" of precipitation input, mixing and rewetting; and (2) to understand the soil water storage capacity and influencing factors of four vegetation areas in mountainous areas.

2. Study area

The Xiying River originates from Lenglongling and Kawazhang in the eastern Qilian Mountains (101°40′47″~102°23′5″E, 37°28′22″~38°1′42″N) (Fig. 1). As the largest tributary of the Shiyang River, it is formed by the Shuiguan River, Ningchang River, Xiangshui River, and Tatu River converging from southwest to northeast and ultimately flows into the Xiying Reservoir. The average annual runoff of the Xiying River is 388 million m^3, which is mainly replenished by mountain precipitation and melting water of ice and snow. The runoff is mainly concentrated in summer. The basin elevation is between 2000 m and 5000 m, corresponding to a temperate semiarid climate with strong solar radiation, a long sunshine time, and a large temperature difference between day and night. The average annual temperature of the basin is 6°C, the annual average evaporation is 1133 mm, the annual average precipitation is 400 mm, and the precipitation from June to September accounts for 69% of the annual precipitation. Precipitation increases with elevation, while temperature decreases with elevation in this area, (Table 1) (Ma et al., 2018). The zonal differentiation of vegetation in the basin is dominated by deciduous forest, mountain grassland, cold temperate coniferous forest, and alpine meadow. The soils mainly include lime, chestnut, alpine shrub meadow, and desert soil (Fig. 1).

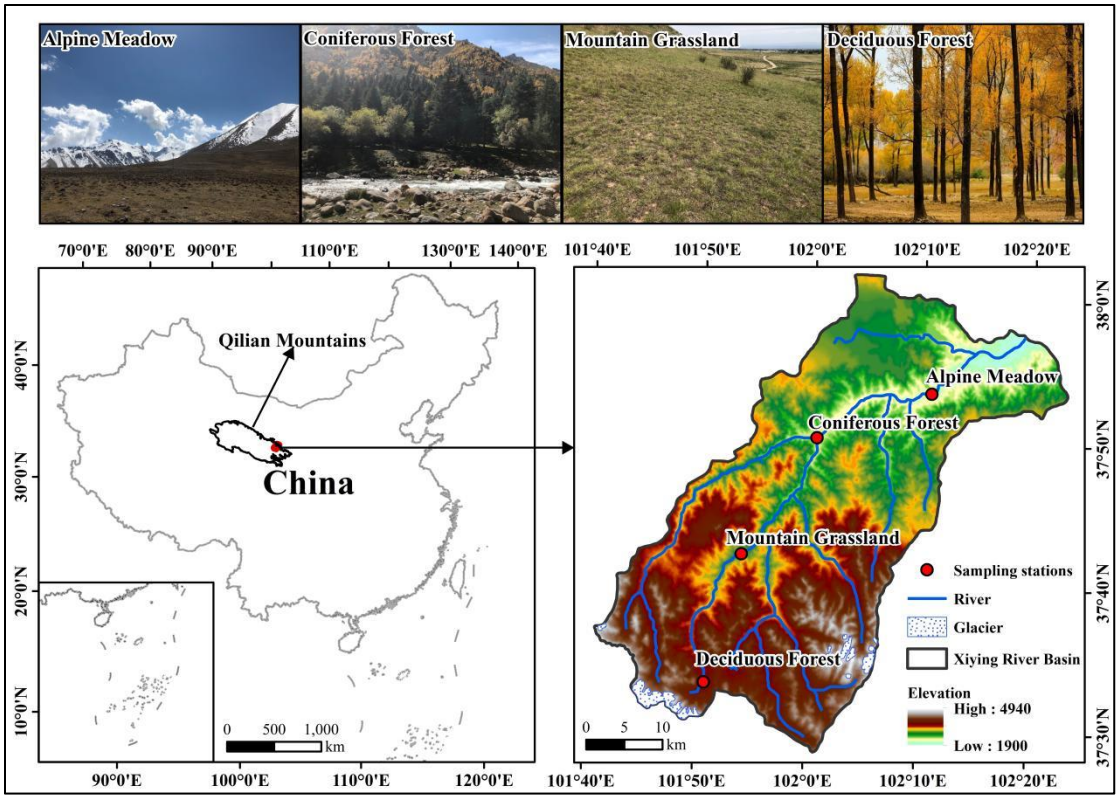

Fig. 1 Study area and location of sampling points

3. Data and methods

3.1 Sample collection

In this study, soil water and precipitation samples were collected from four vegetation zones in the Xiying River Basin from April to October in 2017 (plant growing season). In 2017, the precipitation in the alpine meadows, coniferous forests, mountain grasslands and deciduous forests was 595.1 mm, 431.9 mm, 363.5 mm and 262.5 mm, respectively. The average daily temperatures in the alpine meadows, coniferous forests, mountain grasslands and deciduous forests were -0.19℃, 3.34℃, 6.6℃ and 7.9℃, respectively (Table 1).

Collection of soil samples: Soil samples were collected once a month at depths of 0-10, 10-20, 20-30, 30-40, 40-50, 50-60, 60-70, 70-80, 80-90, and 90-100 cm from the soil layers in the four vegetation zones. Three duplicate samples were collected for each soil layer. A collected soil sample was placed into a 50 mL glass bottle, and the bottle mouth was sealed with Parafilm marked with the sampling date; the sample was then frozen for storage until experimental analysis. Each sample was collected separately in an aluminum box.

Collection of precipitation samples: The precipitation samples were collected by a plastic funnel bottle device. After each precipitation event, the collected precipitation samples were immediately transferred to an 80 mL high-density polyethylene bottle, and the bottle mouth of the samples was sealed with Parafilm; these samples were also frozen and stored until experimental analysis.

Meteorological data: During the sampling period, the local meteorological data were obtained and recorded by automatic weather stations (Watchdog 2000 series weather stations) set up near the sample plot.

Table 1 Basic data of each Vegetation zone from April to October 2017 (*Long*-Longitude, *Lat*-Latitude, *Alt*-Altitude, *T*-Air Temperature (daily mean temperature), *P*-Precipitation (total precipitation during the observation period), *h*-Relative Humidity (daily mean relative humidity))

Vegetation zone	Geographical parameter			Meteorological parametes			Number of samples	
	Long(°E)	*Lat*(°N)	*Alt*(m)	*T*(℃)	*P*(mm)	*h*(%)	Precipitation	Soil
Alpine Meadow	101°51'16"	37°33'28"	3637	-0.19	595.1	69.2	72	47
Coniferous Forest	101°53'23"	37°41'50"	2721	3.34	431.9	66.6	42	41
Mountain Grassland	102°00'25"	37°50'23"	2390	6.6	363.5	60.4	37	54
Deciduous Forest	102°10'56"	37°53'27"	2097	7.9	262.5	59.8	40	53

3.2 Sample determination

The analysis of δ^2H and $\delta^{18}O$ values of all the above water samples was completed using a liquid water isotope analyzer (DLT-100, Los Gatos Research, USA) in the stable isotope laboratory of Northwest Normal University. Before analyzing the isotope values of soil water, the soil water was extracted from the collected soil samples by a low-temperature vacuum condensation system (LI-2100, LICA United Technology Limited, China). Both the water and isotope standard samples were injected 6 times during the analysis. To avoid the "memory effect" of isotope analysis, we discarded the first two injection values and used the average value of the last four injections as the final result (Penna et al., 2012; Qu et al., 2020). The analysis results were relative to VSMOW (Vienna Standard Mean Ocean Water):

$$\delta = \left(\frac{R_{\text{sample}}}{R_{\text{standard}}} - 1 \right) \times 1000‰ \quad (1)$$

where R_{sample} is the ratio of $^{18}O/^{16}O$ or $^{2}H/^{1}H$ in the sample and $R_{standard}$ is the ratio of $^{18}O/^{16}O$ or $^{2}H/^{1}H$ in the VSMOW. The test error of the $\delta^{2}H$ value does not exceed ±0.6‰, and the test error of the $\delta^{18}O$ value does not exceed ±0.2‰.

3.3 Analysis method

3.3.1 Lc-excess

The linear relationship between $\delta^{2}H$ and $\delta^{18}O$ in precipitation and soil water is defined as the LMWL (local meteoric water line) and SWL (soil waterline), respectively, are of great significance for studying the evaporative fractionation of stable isotopes during the water cycle. We further calculated the line-conditioned excess for each soil water and precipitation sample. The lc-excess in different water bodies can characterize the evaporation index of different water bodies relative to the local precipitation (Landwehr and Coplen, 2006).

$$\text{lc}-\text{excess} = \delta^{2}\text{H} - a \times \delta^{2}\text{H} - b \quad (2)$$

where a and b are the slope and intercept of the LMWL, respectively, and $\delta^{2}H$ and $\delta^{18}O$ are the isotopic values of hydrogen and oxygen in the sample. The physical meaning of lc-excess is expressed as the degree of deviation of the isotope value in the sample from the LMWL, indicating the nonequilibrium dynamic fractionation process caused by evaporation. Generally, the change in lc-excess in local precipitation is mainly affected by different water vapor sources, and the annual average is 0. Since the stable isotopes in soil water are enriched by evaporation, the average lc-excess is usually negative (Landwehr et al., 2014; Sprenger et al., 2017).

3.3.2 Potential evapotranspiration

The potential evapotranspiration was calculated based on the Penman-Monteath equation (Allen et al., 1998):

$$\text{PET} = \frac{0.408\Delta(R_n - G) + \gamma \frac{900}{T+273} u^{2}(e_s - e_a)}{\Delta + \gamma(1 + 0.34u^{2})} \quad (3)$$

where PET is the daily potential evapotranspiration (mm day^{-1}), R_n is the net radiation (MJ m^2 day^{-1}), G is the soil heat flux density (MJ m^2 day^{-1}), γ is the psychrometric constant (kPa℃$^{-1}$), u_2 is the wind speed at 2 m height (m s^{-1}), T is the mean daily air temperature at 2 m height (℃), Δ is the slope of the vapor pressure curve (kPa℃$^{-1}$), e_a is the actual vapor pressure (kPa) and e_s is the saturated vapor pressure (kPa). These data come from nearby weather stations.

3.3.3 Soil water storage

Soil water storage is the thickness of the water layer formed by all the water in a certain soil layer (Milly, 1994) and is expressed by the following formula:

$$S = R \times W \times H \times 10 \quad (4)$$

where S is the soil water storage in a certain thickness layer (mm), R is the soil bulk density (g cm^{-3}), and H is the soil thickness (cm). W is the gravimetric water content, which is expressed by the following formula:

$$W = \frac{M_1 - M_2}{M_2} \times 100\% \quad (5)$$

in the formula, M_1 is the gravimetric value of wet soil (g), and M_2 is the gravimetric value of dry soil (g).

4. Results and analysis

4.1 Hydrological climate

PET and runoff are important indicators that reflect the dry-wet conditions of river basins. During the study period (April-October 2017), in the Xiying River Basin, the potential evapotranspiration was 872.8 mm, the daily evapotranspiration ranged from 7.5 mm (July 14) to 0.9 mm (October 9), showing a fluctuating trend around July, and the PET value in April-July was higher than that in August-October. The input of summer precipitation and ice/snow meltwater increased runoff, resulting in a trend similar to PET. During the observation period, the total runoff was 3.1×10^9 m, accounting for 89% of the annual runoff. The variation range of the daily runoff was 286848 m^3 (April 17) to 6125760 m^3 (July 13). The basin before July was drier than that after July (Fig. 2).

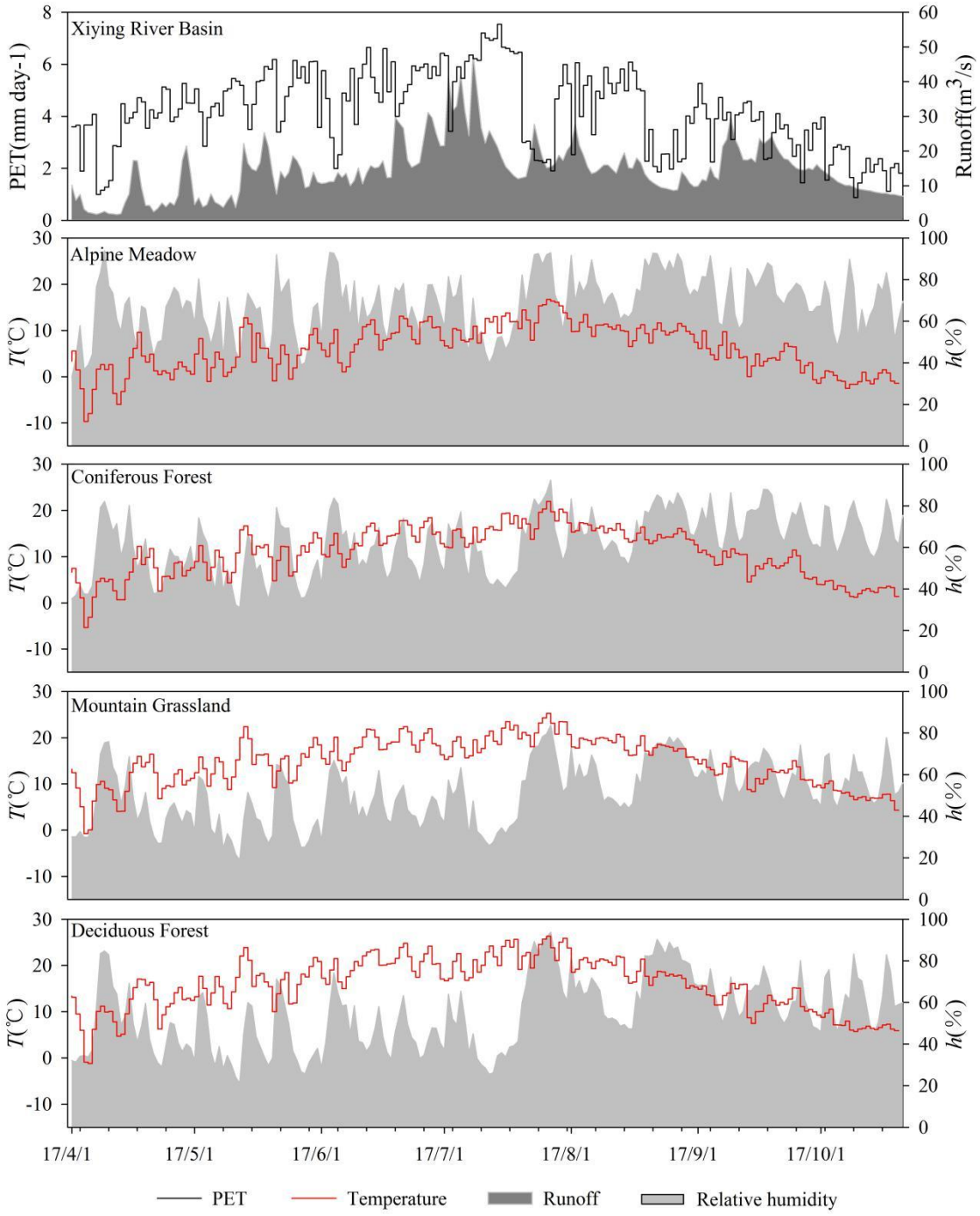

Fig. 2 Climatic and hydrological conditions of Xiying River basin and its vegetation zones

To explore the differences in the natural environment in different vegetation zones, air temperature, atmospheric humidity, and precipitation were used to indicate each research site's temperature and moisture conditions. The hilltop is a typical alpine meadow zone, with a daily average temperature of 6.1°C, ranging from -9.7°C

(April 5) to 16.8°C (July 27). The daily average humidity was 68.2%, with little difference in different periods. During the observation period, there were 72 precipitation events in the alpine meadow zone, and the total precipitation was 534.3 mm, which was relatively evenly distributed each month. In the coniferous forest zone, the daily average temperature during the study period was 10.9°C, ranging from -5.4°C (April 5) to 22.0°C (July 27). The daily average humidity was 62.5%, and the precipitation was 400.6 mm, mainly concentrated from early August to late September. Close to the foothills is the mountain grassland zone, with a daily average temperature of 14.9°C, ranging from -0.7°C (April 5) to 25.3°C (July 27). The average daily humidity was 51.1%, and the precipitation of the vegetation zone during the observation period was 327.2 mm, mainly from late July to mid-August. During the observation period, the daily average temperature in the deciduous forest zone was 15.8°C, ranging from -1.2°C (April 6) to 26.3°C (July 27). The daily average humidity was 54.7%, and the total precipitation was 250.6 mm, which was concentrated in the month from late July to late August. The temperatures of the studied regions were ordered as follows: AM (alpine meadow) < CF (coniferous forest) < MG (mountain grassland) < DF (deciduous forest). The humidities of the studied regions were ordered as follows: AM > CF > MG > DF (Fig. 2).

4.2 Temporal variation in water stable isotopes in different vegetation zones

Influenced by different water sources and complex weather conditions in the precipitation process, the isotopic compositions of precipitation in the four vegetation zones were different during the study period. The mean values of δ^2H and $\delta^{18}O$ in the alpine meadow zone (number of samples: 72) were -73.1‰±36.3‰ (-163.9~13.7‰) and -10.0‰±4.3‰ (-23.1~-1.3‰), respectively. The average δ^2H and $\delta^{18}O$ values of the coniferous forest zone (number of samples: 42) were -42.0‰±37.2‰ (-117.8~13.0‰) and -7.1‰±4.7‰ (-17.4~-0.1‰), respectively. The average δ^2H and $\delta^{18}O$ values of the mountain grassland zone (number of samples: 37) were -37.4‰±30.5‰ (-103.1~4.2‰) and -5.9‰±3.9‰ (-15.1~-0.9‰), respectively. The average δ^2H and $\delta^{18}O$ values of the deciduous forest zone (number of samples: 40) were -31.8‰±42.8‰ (-110.2~23.2‰) and -5.8‰±5.5‰ (-15.2~3.2‰), respectively

(Table 2). The maximum isotopic values of the four vegetation zones appeared on August 4 (AM: 13.7‰, δ^2H; -1.3‰, $\delta^{18}O$), August 10 (CF: 13.0‰, δ^2H; -0.1‰, $\delta^{18}O$), August 7 (MG: 4.2‰, δ^2H; -0.9‰, $\delta^{18}O$) and August 13 (DF: 23.2‰, δ^2H; 3.2‰, $\delta^{18}O$). The highest temperature in each vegetation zone appeared on July 27. The high temperature caused the precipitation to undergo strong below-cloud evaporation during the fall, leading to the enrichment of isotopes. In addition, the atmospheric precipitation isotopes of the four vegetation zones had similar temporal variations: from April to August, the fluctuations in δ^2H and $\delta^{18}O$ increased, reached the maximum in mid-August, and then gradually decreased (Fig. 3).

Table 2 General characteristics of precipitation δ^2H and $\delta^{18}O$ in different vegetation areas from April to October 2017

Vegetation zone	δ^2H/‰				$\delta^{18}O$/‰			
	Max	Min	mean	SD	Max	Min	mean	SD
AM	13.7	-163.9	-73.1	36.3	-1.3	-23.1	-10.0	4.3
CF	13.0	-117.8	-42.0	37.2	-0.1	-17.4	-7.1	4.7
MG	4.2	-103.1	-37.4	30.5	-0.9	-15.1	-5.9	3.9
DF	23.2	-110.2	-31.8	42.8	3.2	-15.2	-5.8	5.5

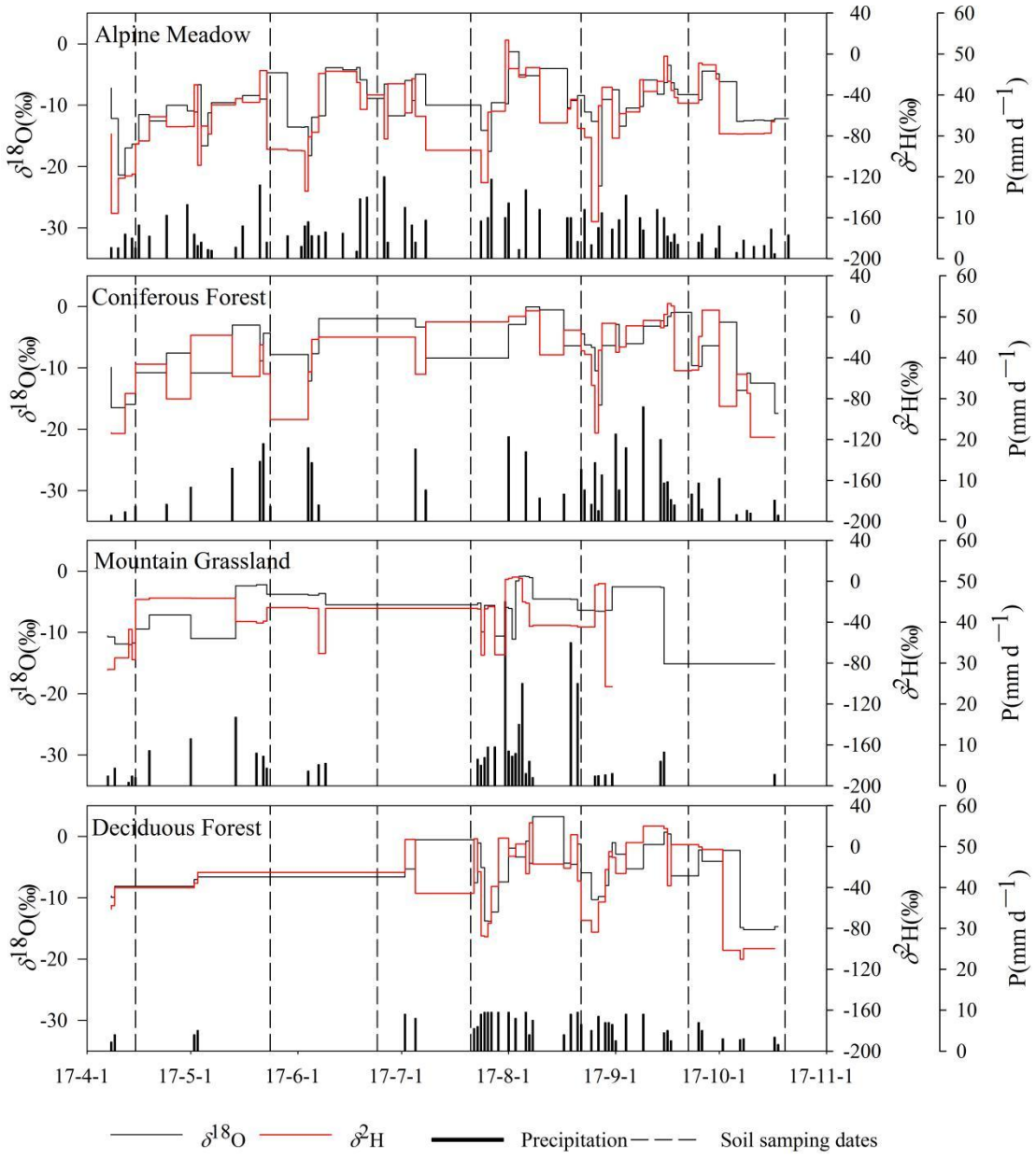

Fig. 3 Time series of rainfall and isotope characteristics in different vegetation zones in Xiying River Basin, with dotted lines indicating the date of soil water sampling

The monthly variation in soil water isotopes records the signal of precipitation input and evaporation. The low-temperature environment and abundant precipitation events in the alpine meadows make the monthly average δ^2H and $\delta^{18}O$ of soil water more depleted than other vegetation zones (-69.4~-51.6‰, δ^2H; -7.5~-10.3‰, δ^2H). Despite this, the SWlc-excess of most samples at this station was still negative, and there were different degrees of evaporation in the process of precipitation penetrating

the soil and mixing with original pore water, among which evaporation fractionation was stronger in July (-11.9‰ lc-excess) and October (-14.5‰ lc-excess). The soil water isotopes of the coniferous forests gradually changed seasonally. From April to July, precipitation was scarce, the temperature rose, and the isotopes of soil water were gradually enriched on the surface (-52.7~-29.5‰, δ^2H; -7.0~-2.1‰, δ^2H), reaching the peak value of the observation period in July (-29.5‰, δ^2H; -2.1‰, $\delta^{18}O$), and continuous rainfall input from late July to mid-August resulted in soil water isotope depletion (-57.0‰, δ^2H; -8.1‰, $\delta^{18}O$). SWlc-excess was an obvious fractionation signal opposite to the trend of isotope change, reaching the lowest value (-26.3‰) in the sampling period in July, and the change in air temperature and precipitation controlled the evaporation intensity. From April to July, the isotopic value of surface soil water in the mountain grasslands was higher ($\delta^{18}O$ was greater than zero), and SWlc-excess was lower than -30‰. During this period, the evaporation and fractionation of shallow soil water were intense. Similar to in the coniferous forests, in the mountain grasslands, the input of heavy precipitation from late July to mid-August led to the depletion of soil water isotopes. There was only sporadic rainfall in the deciduous forests from April to July, and the soil water isotopes were gradually enriched on the surface (-46.1~-18.2‰, δ^2H; -4.7~0.2‰, δ^2H), reached a peak in June when there was no rainfall event (-18.2‰, δ^2H; 0.2‰, $\delta^{18}O$), and then became depleted (-53.2‰, δ^2H; -5.2‰, $\delta^{18}O$). In addition, due to the influence of the Xiying Reservoir and vegetation coverage, the isotopic enrichment degree of soil water in this vegetation zone was lower than that in the mountain grasslands. As the most intuitive form of water change, the gravimetric water content was always at a low value in July (AM: 21.0; CF: 14.8; MG: 11.9; DF: 14.9), when the evaporation was the strongest, and it was most obvious in shallow soil (Table 3) (Fig. 4).

287 **Table 3** General characteristics of soil water δ^2H, $\delta^{18}O$, lc-excess and GWC in different

288 vegetation areas from April to October 2017

Month	Vegetation zone	δ^2H/‰			$\delta^{18}O$/‰			lc-excess/‰			GWC/%		
		Max	Min	Mean	Max	Min	Mean	Max	Min	Mean	Max	Min	Mean
4	AM	-55.2	-70.7	-65.6	-8.5	-10.8	-10.1	-2.7	-7.1	-4.7	25.9	23.0.0.	24.7
	CF	-52.7	-72.2	-63.9	-7.0	-9.9	-8.9	-4.0	-12.0	-8.4	27.6	14.9	20.0
	MG	-7.32	-50.6	-41.0	2.8	-5.8	-3.9	-8.8	-36.8	-19.4	21.7	6.5	14.7
	DF	-46.1	-69.4	-62.1	-4.7	-9.9	-8.5	-2.5	-23.2	-9.7	27.7	19.4	21.8
5	AM	-46.1	-76.5	-66.4	-7.4	-12.2	-10.1	-2.6	-7.7	-4.9	32.6	23.2	28.9
	CF	-45.8	-61.9	-53.5	-5.3	-8.4	-7.0	-9.3	-17.7	-13.0	22.6	9.0	16.1
	MG	-6.7	-47.3	-39.2	2.9	-6.5	-4.3	-4.5	-36.2	-14.4	15.7	7.6	11.2
	DF	-30.8	-63.5	-53.8	-1.9	-9.4	-6.9	-3.2	-30.1	-13.6	26.0	11.7	17.7
6	AM	-62.5	-83.9	-69.4	-8.9	-12.6	-10.3	-1.5	-8.4	-5.8	33.3	21.9	26.0
	CF	-45.8	-78.4	-58.7	-5.1	-12.0	-7.8	5.5	-26.6	-8.5	32.1	10.0	21.3
	MG	-19.7	-74.9	-46.9	0.8	-11.8	-5.8	13.0	-33.7	-11.0	19.3	7.5	14.2
	DF	-18.2	-64.9	-51.7	0.2	-9.0	-5.9	-4.6	-38.2	-19.4	13.5	8.4	11.1
7	AM	-47.3	-60.1	-51.6	-6.9	-8.4	-7.5	-8.8	-14.8	-11.9	25.4	19.0	21.0
	CF	-29.5	-51.4	-41.6	-2.1	-7.9	-5.6	-2.6	-26.3	-11.2	24.3	7.2	14.8
	MG	-10.6	-48.4	-39.2	2.3	-6.4	-4.1	-5.8	-35.8	-16.1	18.7	6.3	11.9
	DF	-35.1	-69.0	-54.1	-1.7	-8.7	-5.5	-14.8	-35.3	-24.5	18.2	11.8	14.4
8	AM	-58.5	-80.3	-66.6	-8.4	-11.6	-9.6	-6.1	-15.4	-9.7	28.1	19.5	25.1
	CF	-57.0	-75.5	-66.4	-8.1	-9.8	-9.2	-2.5	-13.1	-8.3	21.4	8.7	16.3
	MG	-34.2	-53.8	-44.0	-3.2	-5.5	-4.4	-14.7	-22.6	-18.7	11.3	9.5	10.4
	DF	-53.2	-84.3	-67.6	-5.2	-13.5	-9.2	6.8	-26.1	-9.6	23.6	14.7	20.6
9	AM	-48.0	-79.2	-61.0	-7.8	-11.1	-9.2	-4.3	-10.4	-7.2	29.9	20.3	25.3
	CF	-52.5	-67.7	-60.7	-7.8	-10.1	-8.8	-0.1	-11.3	-6.0	31.3	9.3	20.5
	MG	-32.3	-45.3	-38.8	-3.5	-4.4	-4.0	-9.1	-23.8	-16.5	15.3	9.1	13.0
	DF	-30.5	-77.0	-59.8	-3.1	-11.4	-8.2	-1.8	-19.3	-9.3	25.8	14.7	19.1
10	AM	-42.4	-73.5	-58.9	-6.1	-9.8	-7.9	-12.2	-18.2	-14.5	36.2	25.4	29.5
	CF	-59.1	-66.3	-61.7	-8.8	-10.5	-9.5	5.1	-5.3	-1.5	30.0	16.8	23.1
	MG	-50.3	-66.7	-58.3	-5.6	-8.3	-7.1	-5.5	-18.4	-11.9	18.3	11.4	15.8
	DF	-38.0	-61.8	-48.3	-2.7	-8.2	-4.9	-11.9	-34.8	-23.9	25.5	8.9	17.2

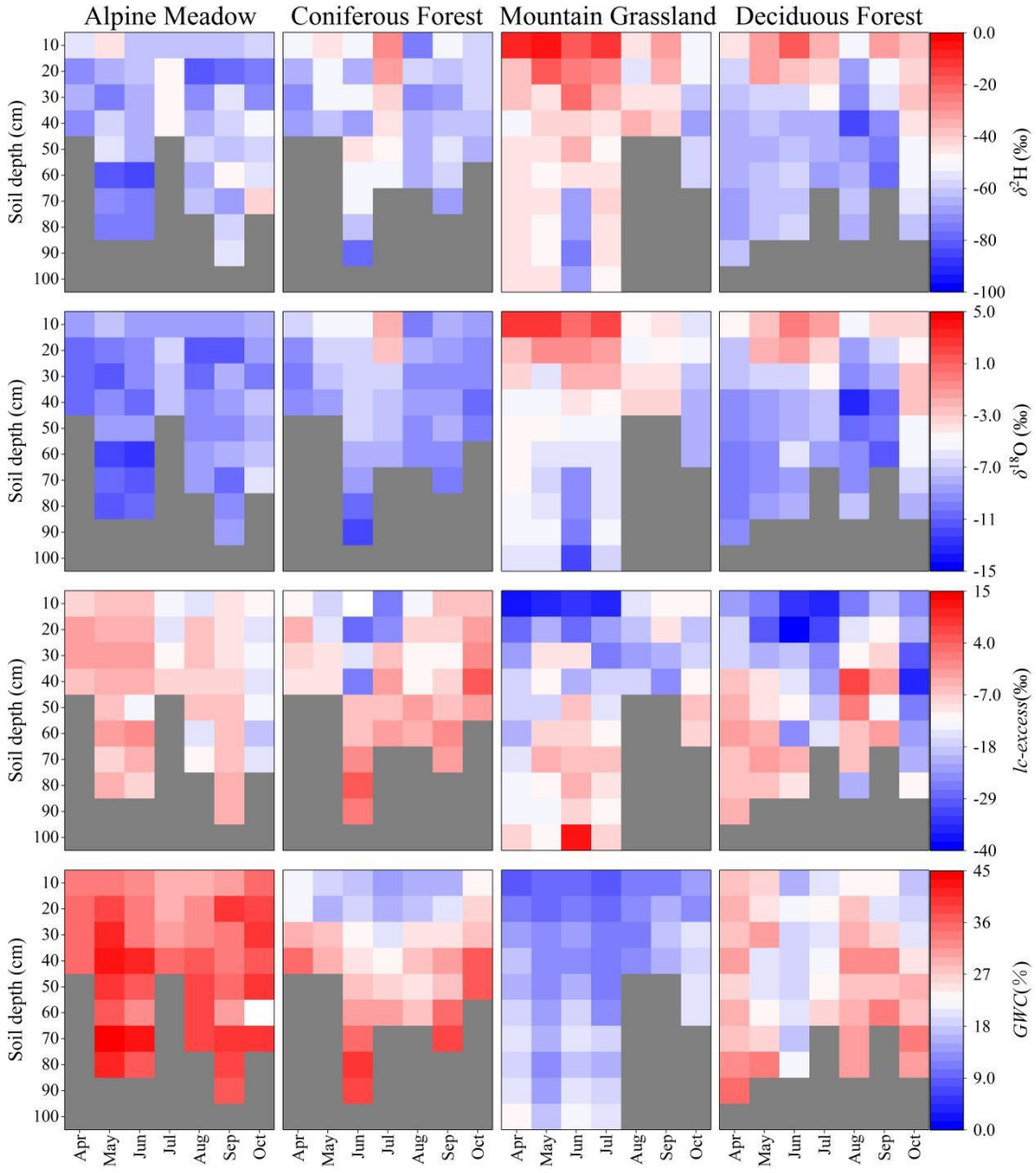

Fig. 4 Heat map of the soil depth profile of δ^2H, $\delta^{18}O$, lc-excess and GWC in different vegetation zones, and the layer lacking measurement is indicated by grey color

4.3 Spatial variation in water stable isotopes in different vegetation zones

Isotope data of precipitation and soil water obtained from different vegetation zones are shown in dual-isotope space in Fig. 5. At the alpine meadow observation station, the slope (8.4) and intercept (23) of the LMWL were higher than those of the GMWL. The slope of the LMWL in the other three vegetation zones was lower than that of the GMWL and gradually decreased with decreasing altitude. With the

decrease in altitude, the slope of the SWL in all vegetation zones except for the deciduous forest SWL decreased (AM: 6.4; CF: 4.7; MG: 3.4; DF: 4.1), indicating that the evaporation of soil moisture increased. On the one hand, the vegetation coverage of the deciduous forest site was higher. On the other hand, the Xiying Reservoir enhanced the regional air humidity and decreased the local water vapor circulation driving force.

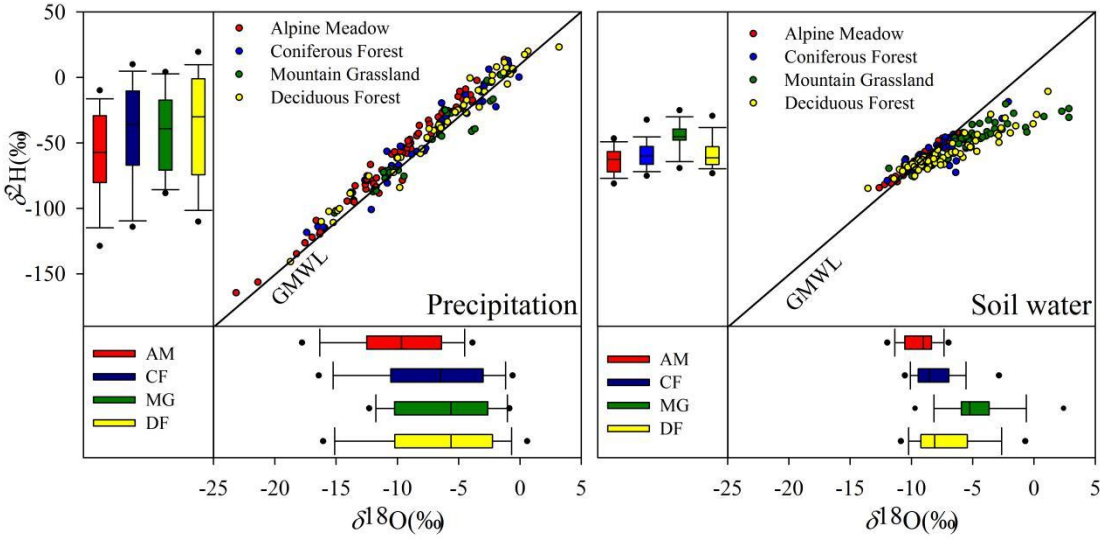

Fig. 5 Dual-isotope space of precipitation (left) and soil water (right) isotope data of four vegetation zones. In the box plots, the box represents 25%-75% percentile, the line in the box represents median (50th percentile), the required line indicates 90th and 10th percentile, and the point indicates the 95th and 5th percentile.

During the study period, compared with that in other vegetation belts, the surface isotopic value of the soil water in the mountain grasslands was relatively enriched (-24.3‰, δ^2H; -0.8‰, $\delta^{18}O$), the lc-excess was smaller and deeper into the middle and lower soil layers (-25.8‰), and the gravimetric water content was relatively low (8.4%). Due to the difference in vegetation types and the influence of reservoirs, this change did not have an obvious elevation effect. Although the elevation was low, the soil water of the deciduous forests had more depleted isotopic characteristics and higher soil moisture than those of the mountain grasslands in most samples. Soil profiles obtained from different vegetation zones can reflect the evaporation signals of water. The low-temperature natural environment made alpine meadow soil less

affected by evaporation (lc-excess > -20‰), and the gravimetric water content was high (gravimetric water content > 20%) during the whole study period. The surface soil water of the coniferous forests was easily affected by climate and had a higher isotopic composition (-29.5‰, δ^2H; -2.1‰, $\delta^{18}O$) and lower lc-excess (-26.3‰). Due to evaporation, soil water isotopes in the mountain grassland and deciduous forest areas were enriched in the surface soil layer. In particular, in the mountain grasslands, the average values of δ^2H and $\delta^{18}O$ in the 0-10 cm soil layer were as high as -24.4‰ and -1.2‰, respectively, and SWlc-excess was lower than -25‰, even close to -40‰ in some samples. In this case, the evaporation signals can easily penetrate the deep soil, making the gravimetric water content values at all the sampling sites lower than 20% (Fig. 4; Fig. 6).

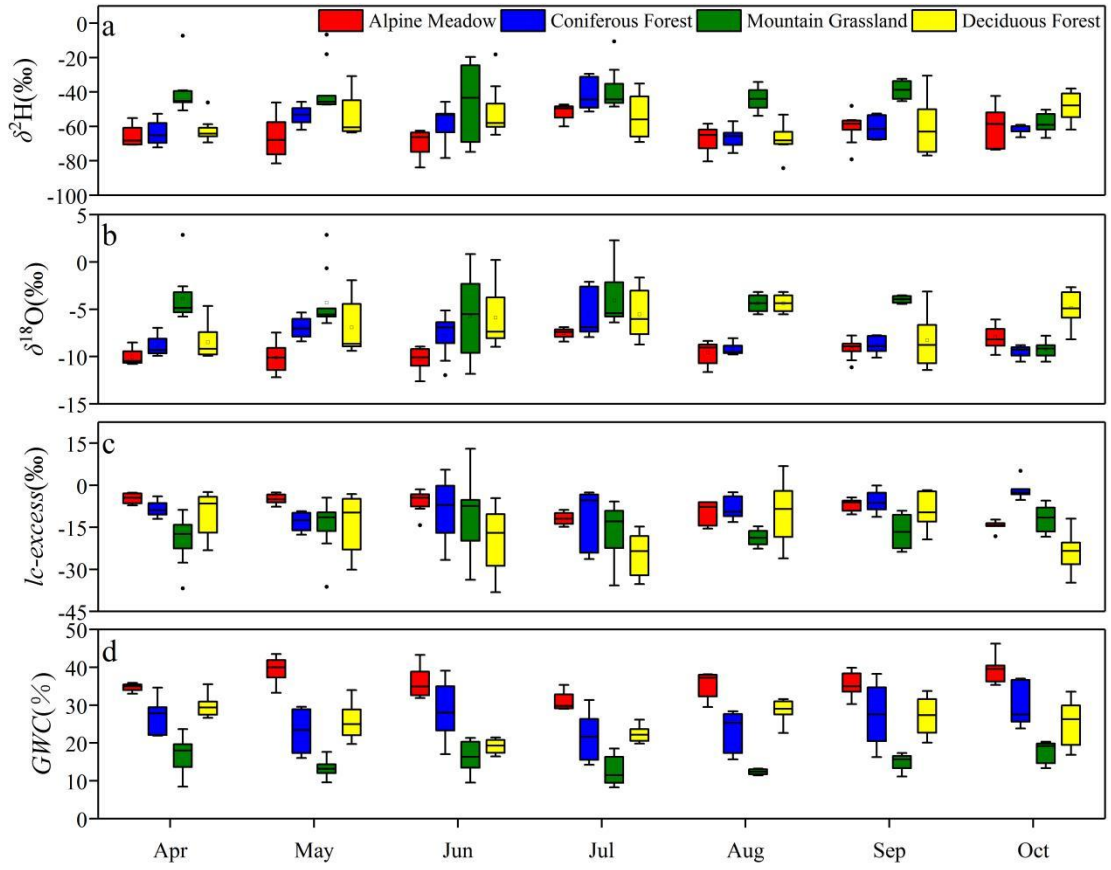

Fig. 6 the variation of δ^2H, $\delta^{18}O$, lc-excess and GWC in different vegetation zones in each sampling

4.4 Variations in the water storage capacity of the 0-40 cm soil layer in different vegetation areas

This study used soil water to calculate the water storage of the 0-40 cm soil layer

in the four vegetation zones during the observation period (Fig 7). The water storage capacity of the alpine meadow gradually decreased from April to July (209.7~167.2 mm), and the water storage capacity increased after July (167.2~201.8 mm). The monthly average water storage capacity was the lowest at 0-10 cm (43.0 mm) and the highest at 30-40 cm (51.7 mm). The water storage capacity of the coniferous forest gradually decreased from April to July (150.1~101.2 mm), and the water storage capacity increased after July (101.2~160.0 mm). The monthly average water storage capacity was the lowest at 0-10 cm (28.0 mm) and the highest at 30-40 cm (40.0 mm). The water storage capacity of the mountain grassland gradually decreased from April to July (80.3~64.0 mm), and the water storage capacity increased after July (64.0~104.6 mm). The monthly average water storage capacity was the lowest at 0-10 cm (17.5 mm) and the highest at 20-30 cm (22.0 mm). The water storage capacity of the deciduous forest gradually decreased from April to June (159.3~104.0 mm), the water storage capacity increased from June to August (104.0~154.0 mm), and there was a decrease from August to October (154.0~111.8 mm). The monthly average water storage capacity was the lowest at 0-10 cm (29.1 mm) and the highest at 20-30 cm (35.0 mm). In general, the soil water storage capacity of the 0-10 cm soil layer was less than that of the other soil layers. The order of the water storage capacity of the 0-40 cm soil layer in the four vegetation zones is AM > DF > CF > MG.

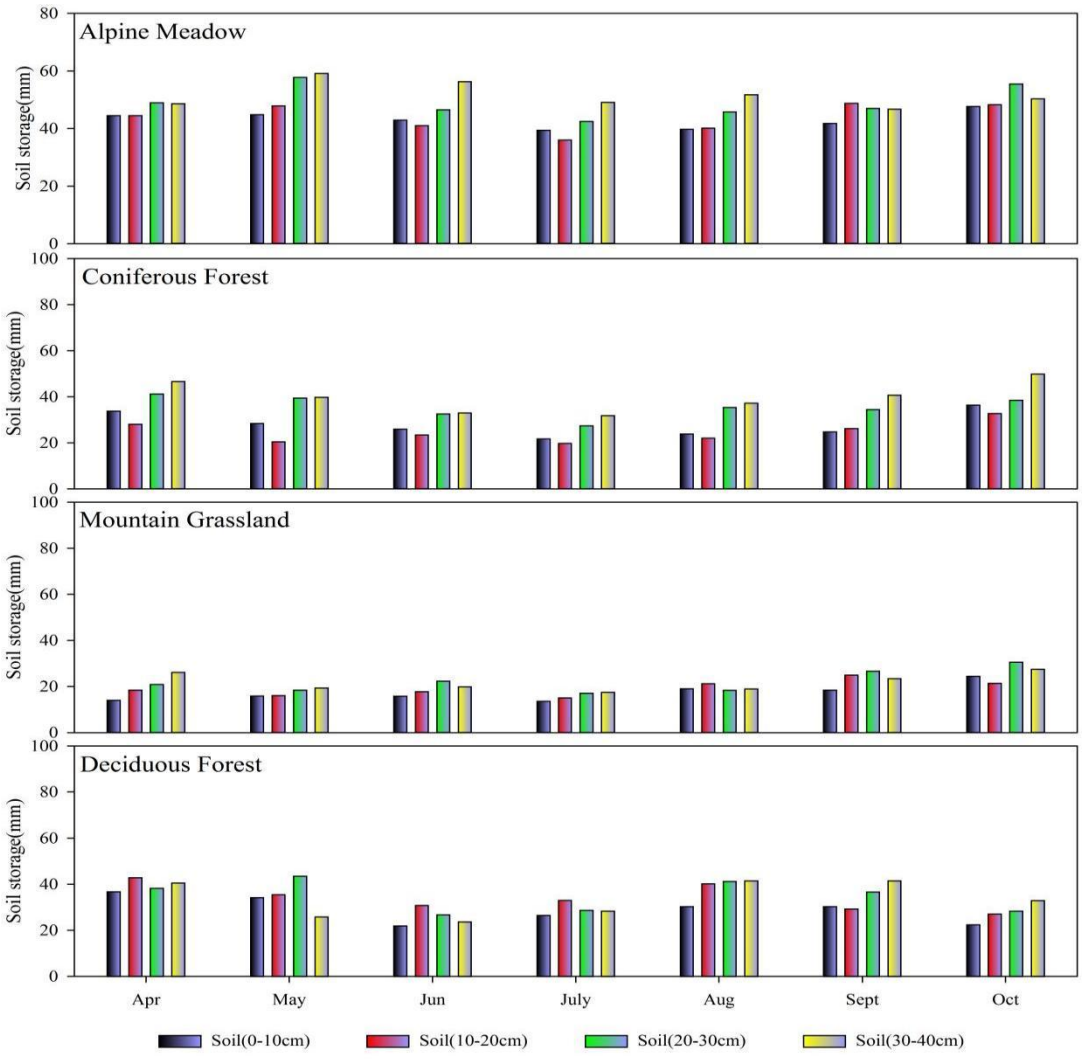

356

357 **Fig. 7** Monthly variation of soil water storage in 0-40cm soil layer of different

358 vegetation zones

359 # 5. Discussion

360 ## 5.1 Evaporation of soil moisture in different vegetation zones

361 In the arid river source area, the replenishment of soil moisture mainly comes

362 from precipitation. The slope of the regional atmospheric precipitation line can reflect

363 the strength of local evaporation. Due to a low atmospheric temperature, low cloud

364 base height, and low air-saturated water vapor loss, the alpine meadow zone was

365 weakly affected by secondary evaporation during precipitation. There, the slope of the

366 LMWL (8.4) was even higher than that of the GMWL (Zhang et al., 2012). As the

367 altitude decreased, the secondary evaporation under clouds strengthened, and the

slope of the LMWL of each vegetation zone decreased (Pang et al., 2011) (Fig 5). The dynamic changes in lc-excess of soil profiles in different vegetation areas reflect the process of soil water evaporation caused by drought during the study period. The monthly average value of SWlc-excess in the alpine meadow zone was less than 0, and the minimum value was -11.9‰ (July). Although the vegetation belt was subject to different degrees of evaporation each month, it was less affected by drought, and it was difficult for evaporation to penetrate into the middle and lower soil layers. The SWlc-excess of the coniferous forest belt was greater than that of the alpine meadow from April to June. The evaporation was the strongest in July (-11.2‰ lc-excess). Similar to in the alpine meadows, in the coniferous forest belt, evaporation mainly occurred in the topsoil. The vegetation coverage of the mountain grassland zone was low, and the arid environment made the isotopes of the surface soil produce strong evaporation signals (lc-excess was close to -40‰). In most samples, the SWlc-excess of the 60-80 cm soil layer was negative. The evaporation signal shifted to the lower layer of the soil (Zimmermann et al., 1966; Barnes and Allison, 1988). Similar evaporation signals have been found in the Mediterranean and arid climate regions (Sprenger et al., 2016b; McCutcheon et al., 2017). Evaporation signals exist in only the surface soil in humid areas, and there is no difference between lc-excess and 0 in the soil layer below 20 cm (Sprenger et al., 2017). The monthly surface soil evaporation of deciduous forests was less than that of mountain grasslands from April to June, and it was greater than that of mountain grasslands after July, mainly due to the influence of the vegetation and reservoirs. There were commonalities in the soil moisture changes in different vegetation zones characterized by more enriched isotopes, stronger evaporation signals, and lower moisture content in the shallow soil. With increasing soil depth, the isotope gradually became depleted, and the evaporation signal was gradually weakened until it disappeared. The evolution of the investigated isotopes, lc-excess, and gravimetric water content in the unsaturated soil showed differences among different vegetation zones. From a high altitude to a low altitude, the isotopic value of the surface gradually increased, and the evaporation signal increased (Fig 4; Fig 6).

5.2 Memory effects of precipitation input, mixing and rewetting

The changes in soil water isotopes and soil moisture can evaluate the input, mixing, and rewetting process of precipitation in different vegetation areas. The main methods of precipitation input are plug flow and preferential flow. Plug flow is the complete mixing of water through the soil matrix with shallow free water. Under the action of plug flow, precipitation infiltrates along the hydraulic gradient, pushing the original soil water downward. Preferential flow means that precipitation uses soil macropores to quickly penetrate shallow soil to form deep leakage (Tang and Feng, 2001). After precipitation, the variability of isotope signals at a certain soil depth can identify the seepage method of water (Peralta-Tapia et al., 2015). During the study period, the soils of the alpine meadow and coniferous forest areas were seasonally frozen and thawed year-round, and the difference in the soil isotope profile was small. The soil moisture profile showed a trend of water increasing from top to bottom, indicating the influence of the previous precipitation. The soil was humid, so the replenishment of soil water by precipitation had the characteristics of top-down piston replenishment. Preferential infiltration showed high variability in isotopic signals (Brodersen et al., 2000), and the rainwater in mountain grasslands and deciduous forests flowed into the deep soil rapidly through the soil matrix via exposed soil fissures and roots. This resulted in the sudden depletion of soil isotopes at a depth of 60-100 cm. This may be due to the more recent depleted precipitation that quickly reached this depth and the preferential infiltration into the soil. Water movement and mixing in the unsaturated zone can be observed in the spatiotemporal variation in isotopes within 1 m of the soil profile, and the alpine meadow and coniferous forest zones underwent considerable rainfall. After a short period of weak evaporation, the soil was rewetted by the next rainfall. In the alpine meadow, the soil moisture remained above 20% each month. The mountain grassland and deciduous forest zones had only sporadic precipitation from mid-May to late July, and the soil moisture evaporated rapidly. With the decrease in air temperature and the occurrence of continuous precipitation after July, the soil was rewetted after two months of drought, and both vegetation zones showed the replacement and mixing of soil water isotopes

and precipitation. The results showed that the soil water storage capacity of the alpine grassland was seriously insufficient, reflecting the incomplete rewetting of the soil by precipitation at the end of the study. In addition, low soil water storage capacity will enrich the remaining soil water isotopes (Zimmermann et al., 1966; Barnes and Allison, 1988). We observed the memory effect of soil rewetting caused by precipitation input and the mixing of different vegetation areas during the entire study period. The changes in soil moisture in each vegetation area reflect different climatic and hydrological characteristics (Fig. 4; Fig. 6).

5.3 Influencing factors of soil water storage capacity in arid headwater areas

As the temperature decreased rapidly with increasing height, precipitation and humidity increased to a certain extent, and the vegetation showed a strip-like alternation approximately parallel to the contour line, forming zonal vegetation with obvious differentiation (Yin et al., 2020). The dry-wet conditions of different vegetation zones restricted the soil water storage capacity in the basin. In the process of low-altitude vegetation zone replacement, the precipitation decreased, the temperature rose, the groundwater level dropped, and the soil water storage capacity was weak (Coussement et al., 2018; Kleine et al., 2020). The soil water storage capacity of the alpine meadow zone with low-temperature and rainy weather was higher than that of other vegetation zones (results of the 0-40 cm soil layers from April to October: AM: 187.8 mm; CF: 128.4 mm; MG: 81.2 mm; DF: 132.1 mm). During the study period, the soil water storage capacity (0-40 cm) exceeded 165 mm each month. With the decrease in altitude, the monthly difference in dry-wet conditions in each vegetation zone gradually became obvious. With the increase in temperature in summer, the environment became dry, and the soil water storage capacity weakened (Sprenger et al., 2017). The soil water storage capacity of the coniferous forest zone began to decrease in April, and the water storage capacity of the 0-40 cm layer reached the minimum value (101.2 mm) in July. The variation in temperature and precipitation was the main reason for the monthly difference (Dubber and Werner, 2019). Although there was a certain water storage capacity in the coniferous forests with some transpiration loss, the soil water storage capacity in

this vegetation zone was not strong. The water storage capacity of mountain grassland soil was lower than that of other vegetation zones. The continuous dry and warm weather in spring and summer led to the water storage capacity of 0-40 cm soil being lower than that of 100 mm every month. In particular, drought stress leads to insufficient soil moisture, making it difficult to maintain plant demand, resulting in sparse vegetation and large-scale exposed surface soil, which further accelerates surface water loss. The continuous precipitation from the end of July prevented further drought development, and the water input gradually restored the soil water storage capacity (Kleine et al., 2020). The deciduous forests had hydrothermal conditions similar to those of the mountain grasslands, but the soil porosity of the forest zone was obviously larger than that of the barren land, and its permeability was higher than that of the barren land. Precipitation infiltrated the ground through roots and turned into groundwater. The forest acted as a reservoir due to its strong water storage and soil conservation capacity (Sprenger et al., 2019). The water storage capacity of the 0-40 cm soil layer in the deciduous forest was higher than 100 mm at each sampling time. In addition, the water content of the 0-40 cm soil layer in each vegetation zone increased with the deepening of the soil layer, and the water storage capacity of the surface soil was weak. The difference in soil properties also led to more water storage in the middle and lower soil layers with higher clay contents (Heinrich et al., 2019) (Fig. 7). Climate warming and the spatiotemporal imbalance of water resources have disturbed the ecological-water balance of different vegetation zones in inland river source areas (Liu et al., 2015). Plant growth mainly depends on the water stored in shallow soil layers (Amin et al., 2020). Drought reduces soil water storage and inhibits plant growth (Li et al., 2020). To effectively improve and manage water resources in arid water source areas, exploring the heterogeneity among different vegetation zones is necessary. According to the basin's current climate, hydrology, and social economy, scientific and reasonable management policies should be formulated according to local conditions for different ecological-hydrological contradictions and extended to more areas.

6. Conclusion

This work provides further insights into the movement and mixing of soil water in different vegetation zones in arid source regions. During the study period, the dynamic changes in lc-excess in the soil profiles of different vegetation zones reflected the evaporation signals caused by drought. Soil water evaporation in spring and summer and insufficient precipitation during the drought period were the main driving forces of isotopic enrichment in the surface soil. The evaporation intensity results of the four vegetation zones followed the order of mountain grassland > deciduous forest > coniferous forest > alpine meadow. In the mountain grassland and deciduous forest zones, drought caused the evaporation signal to penetrate deep into the middle and lower soil layers. The SWlc-excess below 70 cm of the ground surface remained negative. Soil water isotopes and gravimetric water content record the process of soil rewetting caused by precipitation input and mixing. The alpine meadow and coniferous forest zones were enriched in precipitation. After a short period of weak evaporation, the soil was rewetted by the next precipitation event. There was only sporadic precipitation in the mountainous grassland and deciduous forest belt from mid-May to late July. After July, the temperature dropped, and continuous precipitation wet the soil again after two months of drought. The mountain grassland and deciduous forest zones had only sporadic precipitation from mid-May to late July. With the decrease in air temperature and continuous precipitation after July, the soil was rewetted after two months of drought. Moisture and temperature conditions were the key factors that restricted the soil water storage capacity in the different vegetation zones. The soil water storage capacity results followed the order of alpine meadow > deciduous forest > coniferous forest > mountainous grassland. The water storage capacity of the surface soil in each vegetation zone was weak, and more water was stored in the middle and lower soil layers with higher clay contents. This research is helpful to understand the hydrological cycle in different vegetation areas and can provide theoretical support for obtaining a regional ecological hydrological balance.

Reference

Allen, R. G., Pereira, L. S., Raes, D., & Smith, M. (1998). Crop evapotranspiration-Guidelines for computing crop water requirements-FAO Irrigation and drainage paper 56. Fao, Rome, 300(9), D05109.

Amin, A., Zuecco, G., Geris, J., Schwendenmann, L., McDonnell, J. J., Borga, M., & Penna, D. (2020). Depth distribution of soil water sourced by plants at the global scale: A new direct inference approach. Ecohydrology, 13(2), e2177.

Barnes, C. J., & Allison, G. B. (1988). Tracing of water movement in the unsaturated zone using stable isotopes of hydrogen and oxygen. Journal of Hydrology, 100(1-3), 143-176.

Brodersen, C., Pohl, S., Lindenlaub, M., Leibundgut, C., & Wilpert, K. V. (2000). Influence of vegetation structure on isotope content of throughfall and soil water. Hydrological Processes, 14(8), 1439-1448.

Brooks, J. R., Barnard, H. R., Coulombe, R., & McDonnell, J. J. (2010). Ecohydrologic separation of water between trees and streams in a Mediterranean climate. Nature Geoscience, 3(2), 100-104.

Coussement, T., Maloteau, S., Pardon, P., Artru, S., Ridley, S., Javaux, M., & Garré, S. (2018). A tree-bordered field as a surrogate for agroforestry in temperate regions: Where does the water go?. Agricultural Water Management, 210, 198-207.

Dansgaard, W. (1964). Stable isotopes in precipitation. tellus, 16(4), 436-468.

Dubbert, M., & Werner, C. (2019). Water fluxes mediated by vegetation: emerging isotopic insights at the soil and atmosphere interfaces. New Phytologist, 221(4), 1754-1763.

Duvert, C., Stewart, M. K., Cendón, D. I., & Raiber, M. (2016). Time series of tritium, stable isotopes and chloride reveal short-term variations in groundwater contribution to a stream. Hydrology and Earth System Sciences, 20(1), 257-277.

Ferretti, D. F., Pendall, E., Morgan, J. A., Nelson, J. A., Lecain, D., & Mosier, A. R. (2003). Partitioning evapotranspiration fluxes from a Colorado grassland using stable isotopes: Seasonal variations and ecosystem implications of elevated atmospheric CO2. Plant and Soil, 254(2), 291-303.

Gibson, J. J., Holmes, T., Stadnyk, T. A., Birks, S. J., Eby, P., & Pietroniro, A. (2021). Isotopic constraints on water balance and evapotranspiration partitioning in gauged watersheds across Canada. Journal of Hydrology: Regional Studies, 37, 100878.

Grant, G. E., & Dietrich, W. E. (2017). The frontier beneath our feet. Water Resources Research, 53(4), 2605-2609.

Heinrich, I., Balanzategui, D., Bens, O., Blume, T., Brauer, A., Dietze, E., ... & Wille, C. (2019). Regionale Auswirkungen des Globalen Wandels: Der Extremsommer 2018 in Nordostdeutschland. System Erde, 9(1), 38-47.

Hsieh, J. C., Chadwick, O. A., Kelly, E. F., & Savin, S. M. (1998). Oxygen isotopic composition of soil water: quantifying evaporation and transpiration. Geoderma, 82(1-3), 269-293.

Kleine, L., Tetzlaff, D., Smith, A., Wang, H., & Soulsby, C. (2020). Using water stable isotopes to understand evaporation, moisture stress, and re-wetting in catchment forest and grassland soils of the summer drought of 2018. Hydrology and Earth System Sciences, 24(7), 3737-3752.

Koeniger, P., Gaj, M., Beyer, M., & Himmelsbach, T. (2016). Review on soil water isotope-based groundwater recharge estimations. Hydrological Processes, 30(16), 2817-2834.

Landwehr, J. M., & Coplen, T. B. (2006). Line-conditioned excess: a new method for characterizing stable hydrogen and oxygen isotope ratios in hydrologic systems. In International conference on isotopes in environmental studies (pp. 132-135). Vienna: IAEA.

Landwehr, J. M., Coplen, T. B., & Stewart, D. W. (2014). Spatial, seasonal, and source variability in the stable oxygen and hydrogen isotopic composition of tap waters throughout the USA. Hydrological Processes, 28(21), 5382-5422.

Li, X., Piao, S., Wang, K., Wang, X., Wang, T., Ciais, P., ... & Peñuelas, J. (2020). Temporal trade-off between gymnosperm resistance and resilience increases forest sensitivity to extreme drought. Nature Ecology & Evolution, 4(8), 1075-1083.

Liu, Y., Liu, F., Xu, Z., Zhang, J., Wang, L., & An, S. (2015). Variations of soil water isotopes and effective contribution times of precipitation and throughfall to alpine soil water, in Wolong Nature Reserve, China. Catena, 126, 201-208.

573 Ma, X., Jia, W., Zhu, G., Ding, D., Pan, H., & Xu, X. (2018). Stable isotope composition of
574 precipitation at different elevations in the monsoon marginal zone. Quaternary International,
575 493(10), 86-95.
576 McCutcheon, R. J., McNamara, J. P., Kohn, M. J., & Evans, S. L. (2017). An evaluation of the
577 ecohydrological separation hypothesis in a semiarid catchment. Hydrological
578 processes, 31(4), 783-799.
579 Milly, P. C. D. (1994). Climate, soil water storage, and the average annual water balance. Water
580 Resources Research, 30(7), 2143-2156.
581 Pang, Z., Kong, Y., Froehlich, K., Huang, T., Yuan, L., Li, Z., & Wang, F. (2011). Processes
582 affecting isotopes in precipitation of an arid region. Tellus B: Chemical and Physical
583 Meteorology, 63(3), 352-359.
584 Penna, D., Hopp, L., Scandellari, F., Allen, S. T., Benettin, P., Beyer, M., ... & Kirchner, J. W.
585 (2018). Ideas and perspectives: Tracing terrestrial ecosystem water fluxes using hydrogen and
586 oxygen stable isotopes–challenges and opportunities from an interdisciplinary
587 perspective. Biogeosciences, 15(21), 6399-6415.
588 Penna, D., Stenni, B., Šanda, M., Wrede, S., Bogaard, T. A., Michelini, M., ... & Wassenaar, L. I.
589 (2012). Evaluation of between-sample memory effects in the analysis of $\delta^{2}H$ and $\delta^{18}O$ of
590 water samples measured by laser spectroscopes. Hydrology and Earth System Sciences,
591 16(10), 3925-3933.
592 Peralta-Tapia, A., Sponseller, R. A., Tetzlaff, D., Soulsby, C., & Laudon, H. (2015). Connecting
593 precipitation inputs and soil flow pathways to stream water in contrasting boreal
594 catchments. Hydrological Processes, 29(16), 3546-3555.
595 Qu, D., Tian, L., Zhao, H., Yao, P., Xu, B., & Cui, J. (2020). Demonstration of a memory
596 calibration method in water isotope measurement by laser spectroscopy. Rapid
597 Communications in Mass Spectrometry, 34(8), e8689.
598 Rothfuss, Y., & Javaux, M. (2017). Reviews and syntheses: Isotopic approaches to quantify root
599 water uptake: a review and comparison of methods. Biogeosciences, 14(8), 2199-2224.
600 Sharma, H., Ehlers, T. A., Glotzbach, C., Schmid, M., & Tielbörger, K. (2021). Effect of rock
601 uplift and Milankovitch timescale variations in precipitation and vegetation cover on
602 catchment erosion rates. Earth Surface Dynamics, 9(4), 1045-1072.

603 Snelgrove, J. R., Buttle, J. M., Kohn, M. J., & Tetzlaff, D. (2021). Co-evolution of xylem water
604 and soil water stable isotopic composition in a northern mixed forest biome. Hydrology and
605 Earth System Sciences, 25(4), 2169-2186.
606 Sprenger, M., Erhardt, M., Riedel, M., & Weiler, M. (2016a). Historical tracking of nitrate in
607 contrasting vineyards using water isotopes and nitrate depth profiles. Agriculture,
608 Ecosystems & Environment, 222, 185-192.
609 Sprenger, M., Leistert, H., Gimbel, K., & Weiler, M. (2016b). Illuminating hydrological processes
610 at the soil-vegetation-atmosphere interface with water stable isotopes. Reviews of
611 Geophysics, 54(3), 674-704.
612 Sprenger, M., Tetzlaff, D., & Soulsby, C. (2017). Soil water stable isotopes reveal evaporation
613 dynamics at the soil–plant–atmosphere interface of the critical zone. Hydrology and Earth
614 System Sciences, 21(7), 3839-3858.
615 Sprenger, M., Llorens, P., Cayuela, C., Gallart, F., & Latron, J. (2019). Mechanisms of
616 consistently disjunct soil water pools over (pore) space and time. Hydrology and Earth
617 System Sciences, 23(6), 2751-2762.
618 Stumpp, C., Stichler, W., Kandolf, M., & Šimůnek, J. (2012). Effects of land cover and
619 fertilization method on water flow and solute transport in five lysimeters: A long-term study
620 using stable water isotopes. Vadose Zone Journal, 11(1).
621 Tang, K., & Feng, X. (2001). The effect of soil hydrology on the oxygen and hydrogen isotopic
622 compositions of plants' source water. Earth and Planetary Science Letters, 185(3-4), 355-367.
623 Tetzlaff, D., Soulsby, C., Buttle, J., Capell, R., Carey, S. K., Laudon, H., ... & Shanley, J. (2013).
624 Catchments on the cusp? Structural and functional change in northern
625 ecohydrology. Hydrological Processes, 27(5), 766-774.
626 Xiao, W., Wei, Z., & Wen, X. (2018). Evapotranspiration partitioning at the ecosystem scale using
627 the stable isotope method—A review. Agricultural and Forest Meteorology, 263, 346-361.
628 Yin, L. , Dai, E. , Zheng, D. , Wang, Y. , & Tong, M. . (2020). What drives the vegetation
629 dynamics in the hengduan mountain region, southwest china: climate change or human
630 activity?. Ecological Indicators, 112, 106013.

631 Zhang, X. P., Guan, H. D., Sun, Z. A., Sun, G. L., Zhang, X. Z., & Wu, H. W. (2012). Simulations
632 of stable isotopic variations in precipitation and comparison with measured values in Yunnan
633 Province, China. Scientia Geographica Sinica, 32(1), 121-128.
634 Zhu, G., Yong, L., Zhang, Z., Sun, Z., Sang, L., Liu, Y., ... & Guo, H. (2021a). Infiltration process
635 of irrigation water in oasis farmland and its enlightenment to optimization of irrigation mode:
636 Based on stable isotope data. Agricultural Water Management , 258 , 107173.
637 Zhu, G., Yong, L., Zhang, Z., Sun, Z., Wan, Q., Xu, Y., ... & Guo, H. (2021b). Effects of plastic
638 mulch on soil water migration in arid oasis farmland: Evidence of stable isotopes. CATENA ,
639 207 , 105580.
640 Zimmermann, U., Münnich, K. O., Roether, W., Kreutz, W., Schubach, K., & Siegel, O. (1966).
641 Tracers determine movement of soil moisture and evapotranspiration. Science, 152(3720),
642 346-347.

643 **Acknowledgments**

644 This research was financially supported by the National Natural Science
645 Foundation of China (41661005, 41867030, 41971036). The authors much thank the
646 colleagues in the Northwest Normal University for their help in fieldwork, laboratory
647 analysis, data processing.

648 **Author Contribution statement**

649 Guofeng Zhu and Leilei Yong conceived the idea of the study; Yuanxiao Xu and
650 Qiaozhuo Wan analyzed the data; Zhigang Sun and Leilei Yong were responsible for
651 field sampling; Zhuanxia Zhang participated in the experiment; Lei Wang participated
652 in the drawing; Leilei Yong wrote the paper; Liyuan Sang and Yuwei Liu checked and
653 edited language. All authors discussed the results and revised the manuscript.

654 **Additional Information**

655 Competing Interests: The authors declare no competing interests.